ARTICLE

Origin of the Bottlenecks in Preparing Anodized Aluminum Oxide (AAO) Templates on ITO Glass

Thelese R. B. Foong,[†] Alan Sellinger,[‡,§] and Xiao Hu[†,*]

[†]Nanyang Technological University (NTU), School of Materials Science and Engineering, Nanyang Avenue, 639798, Republic of Singapore, and [‡]Institute of Materials Research and Engineering (IMRE), Agency for Science, Technology and Research (A*STAR), 3 Research Link, 117602, Republic of Singapore. [§]Current address: Geballe Laboratory for Advanced Materials, Department of Materials Science and Engineering, Stanford University, 476 Lomita Mall, Stanford, California 94305-4045.

ABSTRACT Nanoporous anodic alumina (AAO) templates are routinely created with ease on substrates, particularly Si wafers. However, the inability to stabilize Al anodization on indium tin oxide (ITO) glass is a key stumbling block that has prevented AAO-assisted deposition of nanomaterial arrays extending from ITO that are attractive for a range of opto-electronic applications (*e.g.*, solar cells and photonic devices). We report on the processing of stable AAO templates directly on ITO substrates by utilizing an ultrathin (0.3 nm) adhesion/passivation layer of Ti between ITO and Al. Precise control of the Ti layer thickness to within the subnanometer (0.2−0.5 nm) range is essential for the anodization process for two factors: (1) to prevent the delamination of Al and destruction of ITO; and (2) to prevent the formation of thick barrier layers at the bottom of the pore channels, which prevent pore connectivity to the conductive ITO substrate. We explore the complex correlation between the electrical properties of substrates (and interlayers) and barrier layer formation and further highlight the criteria for successful barrier layer removal.

KEYWORDS: nanoporous anodic alumina · anodizing Al on ITO glass · barrier layer · electrodeposition

*Address correspondence to asxhu@ntu.edu.sg.

Received for review July 9, 2008 and accepted October 16, 2008.

Published online October 31, 2008.
10.1021/nn800435n CCC: $40.75

Nanostructures such as nanotubes, -rods, and -wires find increasing applications due to their high surface-to-volume ratio, their unique quantum-size-dependent effects, and also the drive to miniaturize computational, electro-optical, and sensing devices.[1,2] To tap into their potential for various applications, it is desirable to develop fabrication methods that (1) allow for good control over the nanostructure dimensions and (2) produce organized arrays of nanostructures on various substrates to facilitate their integration into devices. One such nanostructure that has received tremendous interest is nanoporous anodic alumina (AAO) templates, as it is a simple and inexpensive method for the deposition of a wide range of nanostructures. Unsupported nanorods/wires[3,4] as well as nanorod/wire arrays that protrude vertically from an underlying substrate[5−8] have been fabricated. Furthermore, the anodization of aluminum and the mechanism of pore formation have been reported extensively.[9−14] Generally, when an Al-coated substrate (*e.g.*, Si, glass, Ti-coated substrates) is anodized opposite an inert electrode (Figure 1a) in acidic electrolytes, the aluminum oxide that is formed at the anodizing front contains many surface irregularities where the electric field concentrates. This localized electric field enhances acidic dissolution of the oxide at the bottom of the pores while leaving the pore walls intact, resulting in pore formation (Figure 1b). A thin inverted U-shaped barrier layer produced at the bottom of the pore channels (Figure 1c) is subsequently removed by immersion in dilute acid during which the pores are also enlarged.

AAO templates produced directly on transparent-conductive substrates such as indium tin oxide (ITO)- and fluorine-doped tin oxide (FTO)-coated glasses are desirable as they provide a simple and nonlithographic route to two-dimensional periodic nanoarrays that are useful for a wide range of applications including photonics, photocatalysis, and photovoltaics.[15−17] Though promising in theory, practical implementation of this approach has proven difficult primarily due to the inability to stabilize the Al anodization process on ITO/FTO. Like many conductors (including Pt, Cu, and Ag), ITO/FTO undergo undesirable dissolution and/or oxygen evolution reactions under typical anodization conditions,[5] resulting in the eventual delamination and destruction of the template (see Results and Discussion). To date, only Chu *et al.*[18] have successfully anodized Al on ITO glass. Their achievement could be attributed to the improved physical bonding of AAO to ITO as a result of sputter-depositing high-energy Al atoms on ITO glass. However, sparks and gas evolution were reportedly observed as

the anodization proceeded down to the Al/ITO interface due to isolated anodic dissolution of ITO.[18−20] Furthermore, if anodization was not terminated at the interval prescribed by the authors, the breakdown of ITO induced an increase in ITO sheet resistance to several thousands of ohms, which could be detrimental to the performance of subsequent devices. Other researchers have attached free-standing AAO membranes on ITO using polymeric adhesives.[21,22] However, the use of insulating polymer interlayers is undesirable, particularly in electronic applications.

In this contribution, we report a simple method to produce AAO templates directly on ITO/FTO glass (we use primarily ITO) without the aforementioned problematic issues. The templates are robust and show good adhesion to ITO, while the pore channels are free of barrier layers (through connectivity to ITO surface) (Figure 1c) after a pore widening procedure, making them highly suitable for subsequent nanoarray synthesis. Our methodology involves the interplay of two key experimental variables that ensure successful template formation: (1) an ultrathin (0.3 nm) Ti adhesion and passivation layer between Al and ITO and; and (2) an anodization voltage that approaches the acceptable upper limits of the respective electrolyte (*e.g.*, oxalic, sulfuric acid) system, which favors steady-state pore formation. Templates with undesirably thick barrier layers resulted if the Ti adhesion layer thickness was increase beyond 0.5 nm. Therefore, we elucidate the factors that govern barrier layer thickness and also the mechanisms by which the layer can be effectively removed without affecting the ITO performance.

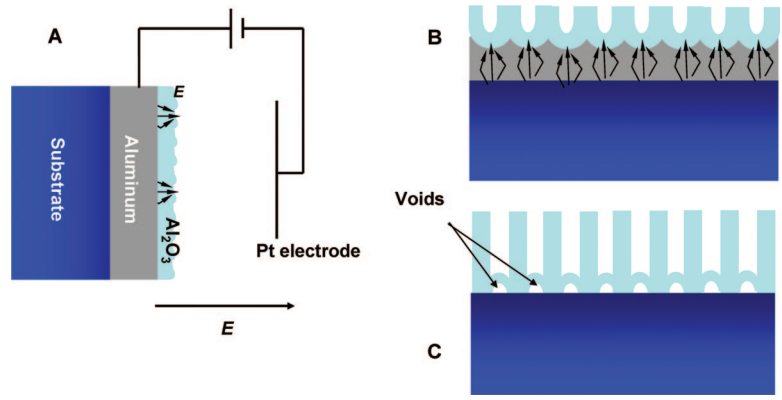

Figure 1. Representation of the processes taking place during anodization (up to the Al−substrate interface) that result in pore formation. (a) Electric field *E* concentrates at surface irregularities of the native aluminum oxide at the anodizing front. (b) Concentrated field enhances acidic dissolution of the oxide at the bottom of the pores, leading to pore channel formation. (c) A thin inverted U-shaped barrier layer is formed when anodization proceeds to and terminates at the substrate.

RESULTS AND DISCUSSION

Anodizing on ITO Glass Substrate. Figure 2 shows chronoamperic curves recorded during the anodization of Al on bare ITO and on ITO coated with thin (10 nm) and ultrathin (0.3 nm) Ti interlayers. The anodization of Al on bare ITO was stable within the first 30 s. However, as the anodizing front approached the Al−ITO interface (beyond 30 s), there was a sudden surge in current, accompanied by sparks, vigorous gas evolution, and template delamination resulting from the anodic breakdown of ITO. We attribute this phenomenon to three main reasons: (1) inadequate adhesion between Al films deposited by thermal or electron-beam evaporation on ITO; (2) compressive forces in the template due to volume expansion as Al is converted to Al_2O_3, which further weaken the template-to-substrate adhesion; and (3) inevitable pinhole defects that are either present intrinsically or are formed during anodization, through which the electrolyte diffuses to the ITO surface, causing localized anodic dissolution of ITO. The breakdown is so vigorous that sparking occurs and gas bubbles produced break through the template, exposing small areas of bare ITO. The dissolution reaction escalates as more areas of ITO are exposed, causing eventual delamination of AAO from ITO.

When a 2−10 nm Ti interlayer (Ti is commonly employed as an adhesion promoter in many applications) was employed, the anodization current was noticeably stabilized (Figure 2), allowing anodization to proceed smoothly down to the substrate (indicated by the current proceeding to zero at 90 s). Unexpectedly, thick ~60 nm barrier layers at the bottom of the AAO pore channels were observed (Figure 3b) after anodization followed by a 45 min pore widening. Since the pore wall and barrier layer are comparable in thickness, prolonged immersion in H_3PO_4 to dissolve the barrier layer also dissolved the template completely. Thick barrier layers are highly undesirable as they render subsequent electro-deposition of materials difficult, if not impossible, and prevent ohmic contact between materials deposited by other vapor or solution techniques and the substrate. The latter is most detrimental to subsequent

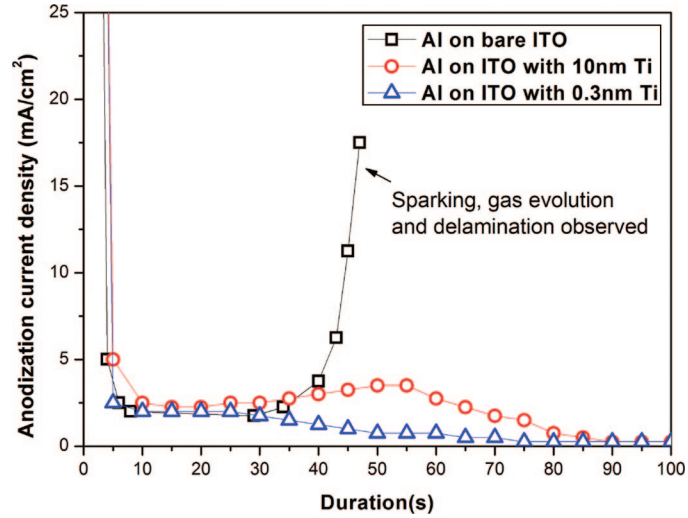

Figure 2. Anodization behavior of Al (~120 nm) coated on various substrates as indicated.

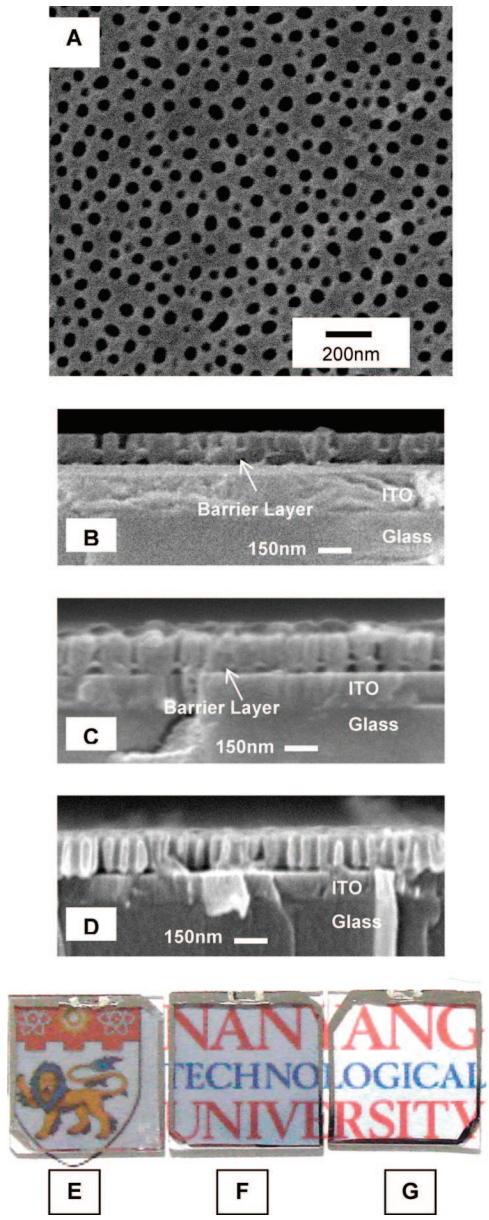

Figure 3. (a) A plan view FESEM image of AAO templates typically produced on ITO coated with 0.3−10 nm Ti. (b) The cross section shows thick ~60 nm barrier layers that remained after a 45 min pore widening process when a 10 nm Ti layer was used. (c) The barrier layers are significantly thinner (~20 nm, after a 20 min pore widening process) when an ultrathin (0.3 nm) Ti was employed. (d) The barrier layers in (c) were removed completely after an additional pore widening duration of 25 min. All templates were produced by anodizing in 0.3 M oxalic acid at 60 V. (e) A small area where AAO had delaminated from the ITO (bottom right corner) is visible in a template anodized at 40 V. Those produced at 60 V were defect free (f and g). Templates without barrier layers (g) are more transparent than those with barrier layers (f).

device integration using such nanoarrays. The formation of thick barrier layers (often as thick as the pore walls) resulting from the use of Ti and other "valve" metals as adhesion layers has been reported in several other publications,[23,24] but to date, there have been no explanations for the observed phenomenon. We have attempted without success a number of methods from literature to thin or eliminate the barrier layer. Liang *et al.*[25] obtained through-hole AAO membranes using reactive ion etching (RIE) to remove the barrier layer, while more recently, Crouse *et al.*[26] introduced an *in situ* barrier layer removal procedure that involved stepping up the voltage at the end of the anodization process (for a materials system involving Si substrate coated with Pt, Ti, and Al, respectively). In our experiments, the RIE treatment tended to be unstable and reduced the total template thickness more than the barrier layer thickness, while the latter approach proved ineffective for our materials system.

We have discovered that significantly thinner barrier layers on the order of 20 nm could be achieved after anodization if the thickness of the initial Ti interlayer is reduced further to the subnanometer (0.2−0.5 nm) level. Figure 3c,d shows that the thin 20 nm barrier layers following 20 min of pore widening were completely dissolved after a further 25 min immersion (*i.e.*, a total pore widening procedure of 45 min), resulting in pore channels that extended through to the ITO. From AFM (Figure 4b), it is apparent that the 0.2−0.5 nm Ti evaporated was not a continuous layer but composed of Ti islands (*ca.* 7−9 nm in diameter) dispersed across the ITO surface. The chronoamperic characteristics (Figure 2) were stable with no evidence of anodic breakdown of ITO or delamination problems. In addition, the anodization process did not deteriorate the electrical properties of ITO. For example, the ITO sheet resistance of 13.6 Ω/sq measured after anodization and template removal (by immersing in 0.1 M KOH for an hour) was marginally increased over that of a pristine ITO substrate (10.3 Ω/sq), compared to the sharp increase in resistance (by 2 orders of magnitude, if the anodization duration was not carefully controlled) reported elsewhere.[20] Ti appears to function remarkably as a passivation/adhesion component, preventing direct contact between ITO and the electrolyte, which is vital to preventing anodic dissolution of ITO during anodization.

To further demonstrate that the AAO templates are robust, show good adhesion to the ITO glass substrate, and are able to support subsequent growth of nanomaterial arrays, we electrochemically deposited Ni under DC bias into the templates with ITO as the working electrode using standard Ni plating apparatus. Straightforward electro-deposition under DC bias is a good indication that the AAO pore channels are unobstructed. We were unable to deposit Ni when templates with thick barrier layers (Figure 3b) were employed. Figure 5a shows a plan view SEM image of a uniform array of Ni nanorods after template removal, while the cross section (Figure 5b) indicates that the nanorods had overgrown the template slightly, resulting in a "nanomushroom" array.

Our procedures for successful barrier-layer-free template formation on ITO glasses are repeatable across

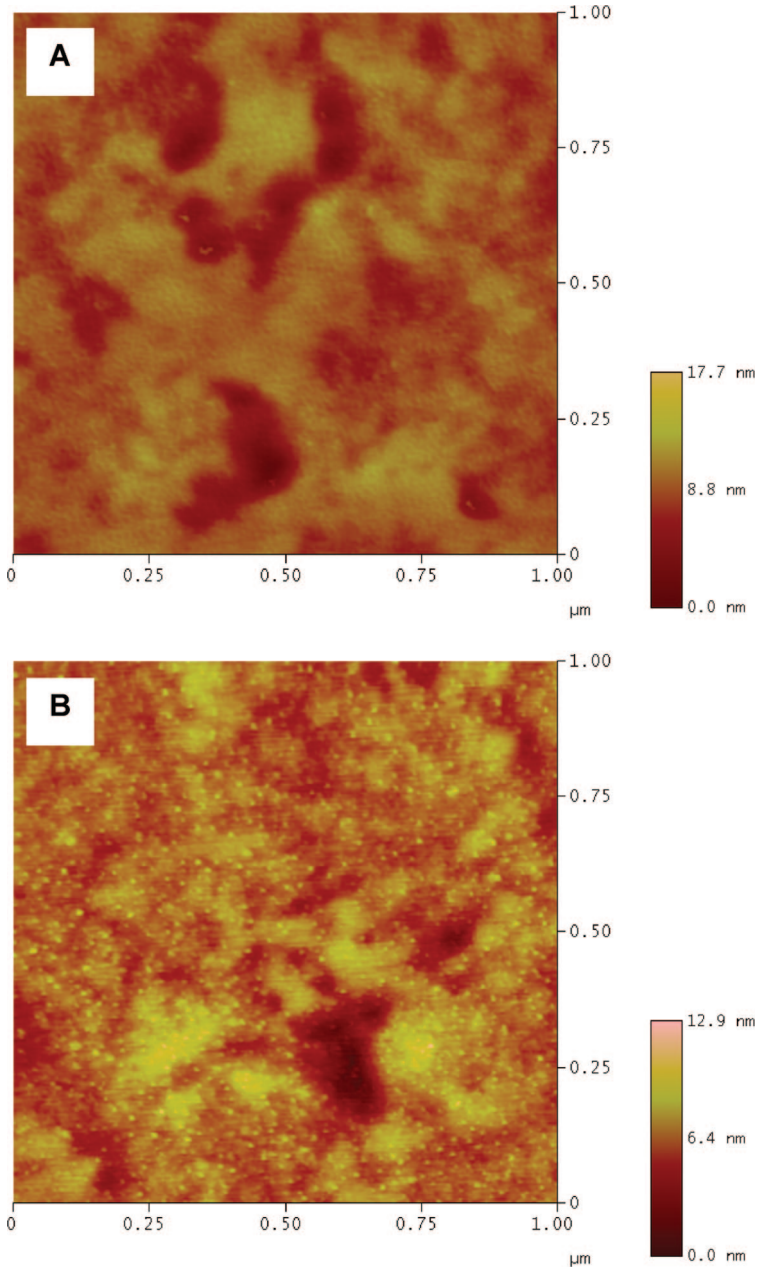

Figure 4. AFM morphology of (a) a blank ITO substrate and (b) an ITO substrate with 0.3 nm Ti evaporated. The ultrathin 0.3 nm Ti layer is not a continuous layer but is composed of small Ti islands.

the anodization voltage range recommended for the various electrolyte systems (*i.e.*, 25−40 V for 0.2 M sulfuric acid and 40−80 V for 0.3 M oxalic acid). However, we propose applying voltages that approach the upper limits of those voltage ranges. Small areas where the template had delaminated slightly from ITO were occasionally observed in templates produced using lower voltages (Figure 3e). The delaminations appear to have manifested from localized breakdown of ITO as a result of the electrolyte diffusing through pinhole defects in the Al film to the ITO during anodization. Increasing the applied voltage accelerates the pore formation process while suppressing defect formation, thereby enhancing the integrity of templates produced (Figure 3f,g). Sixty volts for oxalic and 35 V for sulfuric acids are effective in this regard.

TABLE 1. Details of the Various Insulating and Semiconducting Substrates and Interlayers Prepared To Compare Barrier Layer Formation Characteristics

substrate class	details
insulating	plain glass
	50 nm amorphous TiO_2-coated ITO glass
semiconducting	silicon wafer (p-type, [100]))
	50 nm anatase TiO_2-coated ITO glass

Factors Governing Barrier Layer Thickness, Morphology, and Its Subsequent Removal. To further understand why irremovable barrier layers were observed with thicker

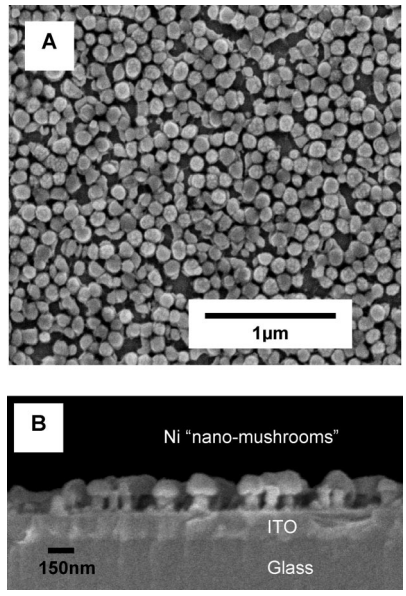

Figure 5. (a) Plan and (b) corresponding cross-sectional FESEM image of Ni nanorods protruding from the ITO.

(2−10 nm) Ti adhesion layers as opposed to ultrathin (0.2−0.5 nm), we attempted to compare the anodization characteristics and corresponding morphologies of AAO templates fabricated from several insulating (plain microscope glass and ITO glass coated with 50 nm of amorphous TiO_2) and semiconducting (Si and ITO glass coated with 50 nm of anatase TiO_2) substrates and interlayers (Table 1). Ti-coated ITO substrates are also categorized under the class of substrates with an insulating interlayer (see Supporting Information for evidence that Ti was converted to amorphous and insulating TiO_2 during anodization). For better comparison, all substrates were coated with the same thickness of Al and were anodized under the same conditions. Interestingly, insulating substrates and interlayers yielded templates with thick barrier layers (Figures 3b and 6c,d), while those produced on semiconductors were barrier-layer-free (Figure 6a,b) after pore widening. Contrary to expectation, the chronoamperic curves recorded from all four substrates (Figure 7) were similar in magnitude and shape, with little obvious differences to explain the trends gathered from FESEM (Figure 6). More in-depth studies (*e.g.*, using the three-electrode setup) may be required to elucidate any correlation between barrier layer formation and the anodization characteristics. Nevertheless, the FESEM images clearly support our hypothesis that barrier layer formation and morphology are governed by the conductivity of the underlying substrate.

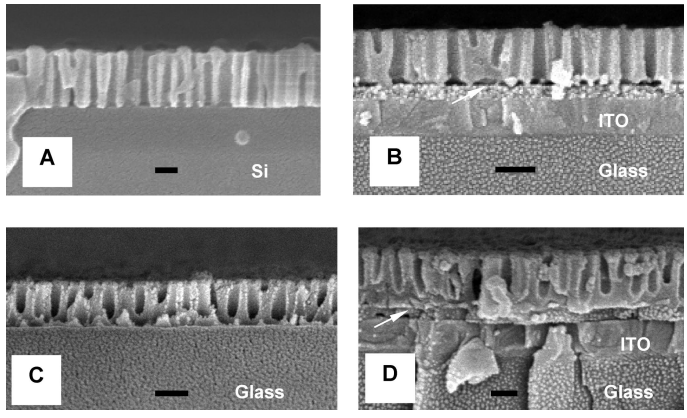

Figure 6. Cross-sectional FESEM images of AAO templates produced on semiconducting (a) Si and (b) anatase TiO_2-coated ITO, and insulating (c) plain glass and (d) amorphous TiO_2-coated ITO. The spin-coated TiO_2 layers in (b) and (d) are indicated by the white arrows. Barrier layers are evident in (c) and (d). All templates underwent a 45 min pore widening etch. All scale bars reflect 150 nm.

It is known that the barrier layers in AAO produced on substrates typically adopt an inverted U-shape. According to Crouse *et al.*,[12] the inverted morphology results from the dissolution of alumina located between the barrier layer and the substrate to form voids (Figure 1c). The more the alumina dissolves, the larger the voids and the thinner the barrier layer. The dissolution of alumina is catalyzed by a localized electric field at the template-to-substrate interface. We postulate that, during anodization, this local field, vital for barrier layer reduction, was significantly reduced (or was even nonexistent) when insulating substrates or insulating interlayers were used. Consequently, glass substrates (Figure 6c) as well as ITO coated with 50 nm amorphous TiO_2 (Figure 6d) and 2−10 nm Ti (Figure 3b) resulted in templates with thick barrier layers. It is also apparent that the morphology of the barrier layer ranges from void (Figure 3b) to void-free (Figure 6d), depending on the thickness of the insulating interlayer. For example, thicker insulating layers require higher electric fields necessary for alumina dissolution while concurrently avoiding void formation. In contrast, their semiconducting counterparts supported a field that was large enough for effective barrier layer thinning. As the resulting barrier layers were sufficiently thin, they were successfully removed during subsequent pore widening (Figure 6a,b). The above arguments also explain why templates produced on ITO coated with 0.2−0.5 nm Ti were barrier-layer-free (after pore widening). Being ultrathin, the Ti interlayer had little influence over the electric field needed for barrier layer reduction.

CONCLUSIONS

We have identified and demonstrated two key elements that are essential to the formation of robust AAO templates on ITO substrates: (1) an ultrathin (~0.3 nm) Ti adhesion layer that effectively prevented destructive anodic breakdown of ITO; and (2) an anodization voltage higher than conventionally applied that reduced defects in the templates. The templates had barrier layers that were thin enough to be eliminated *via* the usual post-pore-widening procedure and were resilient enough to support subsequent growth of Ni nanorods on ITO *via* standard DC electro-deposition. The thick-

ness of the Ti adhesion layer should be carefully confined within the subnanometer (0.2−0.5 nm) regime. Otherwise, thicker Ti, which is converted to amorphous and insulating TiO_2 during anodization, would deplete the electric field required for barrier layer thinning during anodization. When AAO templates fabricated on a series of insulating and semiconducting substrates and interlayers were compared, insulating substrates and interlayers were found to produce thick impenetrable barrier layers. Conversely, semiconducting substrates supported a larger local field that allowed for successful thinning of the barrier layer. The results and relationships established herein clearly emphasize the need for careful substrate selection when template formation by Al anodization is involved. In cases where insulating substrates or interlayers are required, other template-forming techniques (*e.g.*, lithography) could be more appropriate. Future work from our group will explore functionalizing the AAO pore walls and network for application in organic photovoltaics (OPV).[27−29]

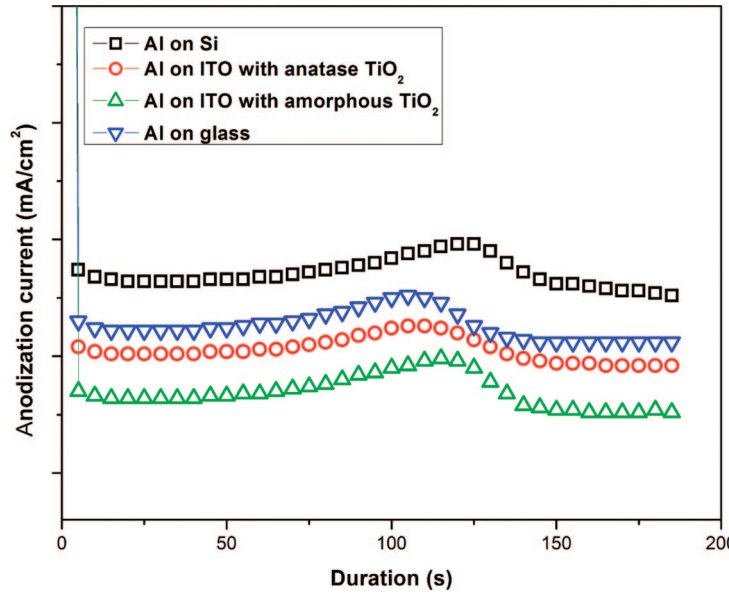

Figure 7. Anodization behavior of Al (~200 nm) coated on various insulating and semiconducting substrates and interlayers. All curves have been arbitrarily shifted for clarity.

EXPERIMENTAL SECTION

Template Preparation on ITO Glass. ITO-coated glass substrates (with sheet resistance of 10.3 Ω/sq obtained from Merck Display Technologies) were cleaned by ultrasonication in detergent, acetone, and IPA. They were then dried with a stream of pressurized N_2 and subjected to O_2 plasma cleaning for 5 min. Pure Al (Super Conductor Materials 99.9999%) films (100−200 nm thick) were deposited onto ITO glass by electron-beam evaporation (Edwards FL400) at a rate of 5 nm/s. Templates with Ti interlayers of different thickness were prepared by evaporating 0.2−10 nm Ti (CERAC Specialty Inorganics 99.995%) at a rate of 0.02−0.04 nm/s prior to Al evaporation without breaking chamber vacuum. The coated substrates were next anodized opposite a platinum mesh counter electrode at 60 V in 0.3 M oxalic or 35 V in 0.2 M sulfuric acid, each maintained at 2 °C. Finally, the anodized films were immersed in 5 wt % H_3PO_4 to adjust the pore diameter and remove the barrier layer.

Anodizing on Other Substrates. Several other types of semiconducting and insulating substrates with and without interlayers (Table 1) were prepared to study the dependence of barrier layer formation on substrate conductivity. All substrates were cut to the same dimensions for fair comparison and were precleaned following procedures described above. TiO_2 layers on ITO glass were spin coated from a solution produced from room temperature acid-catalyzed hydrolysis of titanium(IV) isopropoxide (TIP) in ethanol with a molar ratio of TIP/H_2O/ethanol/HNO_3 = 1:1:50:0.2.[30] The films were then heated at 120 °C for 10 min, resulting in amorphous, insulating TiO_2, and/or annealed further at 500 °C for 2 h in air to obtain crystalline anatase, semiconducting TiO_2. The substrates described above were coated with Al and subjected to anodization.

Electrochemical Deposition of Ni Nanorods in AAO Templates Prepared on ITO. To demonstrate that the AAO templates created were resilient enough to support subsequent deposition of nanomaterial arrays, Ni nanorods were electrochemically deposited through the AAO template onto ITO glass by cathodically polarizing ITO at −0.75 V opposite a platinum mesh counter electrode in a standard three-electrode setup and a commercial Ni plating solution (Hiap Guan Electro-plating Materials). The estimated deposition rate was *ca.* 10 nm/min. Hence the deposition was stopped just before the nanorods overfilled the templates and formed a blanket Ni layer. The AAO template was subsequently etched away in 0.1 M KOH to expose the embedded Ni nanorod array.

Characterization. The AAO template, barrier layer structure, and Ni nanorod arrays were characterized mainly by field-emission scanning electron microscopy (FESEM, JEOL 6700F). Atomic force microscopy (AFM, Digital Instrument's Nanoscope III) was used to investigate the surface morphology of the various substrates employed and measure film thickness. Sheet resistance measurements were taken on the SYS-301 resistivity probing system, Signatone Corporation. X-ray photoelectron spectroscopy (XPS) analyses were conducted on the VG ESCALAB 220I-XL imaging system equipped with a monochromatic Al-α source. The anodization current/voltage characteristics were monitored on a Sorensen power meter.

Acknowledgment. The authors thank Nanyang Technological University (NTU) and the National Research Foundation (NRF), Singapore, for funding this work. Thanks are also due to the Institute of Materials Research and Engineering (IMRE) for extensive usage of laboratory facilities. We gratefully acknowledge Ms. Nelvi Sutanto for her kind assistance in XPS data collection.

Supporting Information Available: Evidence that Ti is converted to amorphous TiO_2 during anodization. This explains why Ti-coated ITO is grouped under the class of insulating substrates. This material is available free of charge *via* the Internet at http://pubs.acs.org.

REFERENCES AND NOTES

1. Appell, D. Nanotechnology: Wired for Success. *Nature* **2002**, *419*, 553–555.
2. Thelander, C.; Agarwal, P.; Brongersma, S.; Eymery, J.; Feiner, L. F.; Forchel, A.; Scheffler, M.; Riess, W.; Ohlsson, B. J.; Gosele, U.; et al. Nanowire-Based One-Dimensional Electronics. *Mater. Today* **2006**, *9*, 28–35.
3. Lakshmi, B. B.; Patrissi, C. J.; Martin, C. R. Sol−Gel Template Synthesis of Semiconductor Oxide Micro- and Nanostructures. *Chem. Mater.* **1997**, *9*, 2544–2550.
4. Yao, B.; Fleming, D.; Morris, M. A.; Lawrence, S. E. Structural Control of Mesoporous Silica Nanowire Arrays in Porous Alumina Membranes. *Chem. Mater.* **2004**, *16*, 4851–4855.

5. Rabin, O.; Herz, P. R.; Lin, Y. M.; Akinwande, A. I.; Cronin, S. B.; Dresselhaus, M. S. Formation of Thick Porous Anodic Alumina Films and Nanowire Arrays on Silicon Wafers and Glass. *Adv. Funct. Mater.* **2003**, *13*, 631–638.
6. Sander, M. S.; Tan, L. S. Nanoparticle Arrays on Surfaces Fabricated Using Anodic Alumina Films as Templates. *Adv. Funct. Mater.* **2003**, *13*, 393–397.
7. Shingubara, S.; Okino, O.; Sayama, Y.; Sakaue, H.; Takahagi, T. Two-Dimensional Nanowire Array Formation on Si Substrate Using Self-Organized Nanoholes of Anodically Oxidized Aluminum. *Solid-State Electron.* **1999**, *43*, 1143–1146.
8. Tan, L. K.; Chong, M. A. S.; Gao, H. Free-Standing Porous Anodic Alumina Templates for Atomic Layer Deposition of Highly Ordered TiO_2 Nanotube Arrays on Various Substrates. *J. Phys. Chem. C* **2008**, *112*, 69–73.
9. Li, A. P.; Muller, F.; Birner, A.; Nielsch, K.; Gosele, U. Hexagonal Pore Arrays with a 50−420 nm Interpore Distance Formed by Self-Organization in Anodic Alumina. *J. Appl. Phys.* **1998**, *84*, 6023–6026.
10. O'Sullivan, J. P.; Wood, G. C. The Morphology and Mechanism of Formation of Porous Anodic Films on Aluminium. *Proc. R. Soc. London, Ser. A* **1970**, *317*, 511–543.
11. Li, F. Y.; Zhang, L.; Metzger, R. M. On the Growth of Highly Ordered Pores in Anodized Aluminum Oxide. *Chem. Mater.* **1998**, *10*, 2470–2480.
12. Crouse, D.; Lo, Y. H.; Miller, A. E.; Crouse, M. Self-Ordered Pore Structure of Anodized Aluminum on Silicon and Pattern Transfer. *Appl. Phys. Lett.* **2000**, *76*, 49–51.
13. Jessensky, O.; Muller, F.; Gosele, U. Self-Organized Formation of Hexagonal Pore Arrays in Anodic Alumina. *Appl. Phys. Lett.* **1998**, *72*, 1173–1175.
14. Masuda, H.; Yasui, K.; Sakamoto, Y.; Nakao, M.; Tamamura, T.; Nishio, K. Ideally Ordered Anodic Porous Alumina Mask Prepared by Imprinting of Vacuum-Evaporated Al on Si. *Jpn. J. Appl. Phys.* **2001**, *40*, L1267–L1269.
15. Teh, L. K.; Furin, V.; Martucci, A.; Guglielmi, M.; Wong, C. C.; Romanato, F. Electrodeposition of CdSe on Nanopatterned Pillar Arrays for Photonic and Photovoltaic Applications. *Thin Solid Films* **2007**, *515*, 5787–5791.
16. Shyue, J. J.; Cochran, R. E.; Padture, N. P. Transparent-Conducting, Gas-Sensing Nanostructures (Nanotubes, Nanowires, and Thin Films) of Titanium Oxide Synthesized at Near-Ambient Conditions. *J. Mater. Res.* **2006**, *21*, 2894–2903.
17. Kim, S. S.; Chun, C.; Hong, J. C.; Kim, D. Y. Well-Ordered TiO_2 Nanostructures Fabricated Using Surface Relief Gratings on Polymer Films. *J. Mater. Chem.* **2006**, *16*, 370–375.
18. Chu, S. Z.; Wada, K.; Inoue, S.; Todoroki, S. Formation and Microstructures of Anodic Alumina Films from Aluminum Sputtered on Glass Substrate. *J. Electrochem. Soc.* **2002**, *149*, B321–B327.
19. Chu, S. Z.; Wada, K.; Inoue, S.; Todoroki, S. Synthesis and Characterization of Titania Nanostructures on Glass by Al Anodization and Sol−Gel Process. *Chem. Mater.* **2002**, *14*, 266–272.
20. Chu, S. Z.; Wada, K.; Inoue, S.; Todoroki, S. Fabrication and Characteristics of Nanostructures on Glass by A1 Anodization and Electrodeposition. *Electrochim. Acta* **2003**, *48*, 3147–3153.
21. Liu, L.; Zhao, Y. M.; Jia, N. Q.; Zhou, Q.; Zhao, C. J.; Yan, M. M.; Jiang, Z. Y. Electrochemical Fabrication and Electronic Behavior of Polypyrrole Nano-fiber Array Devices. *Thin Solid Films* **2006**, *503*, 241–245.
22. Limmer, S. J.; Chou, T. P.; Cao, G. Z. A Study on the Growth of TiO_2 Nanorods Using Sol Electrophoresis. *J. Mater. Sc.* **2004**, *39*, 895–901.
23. Cai, A. L.; Zhang, H. Y.; Hua, H.; Zhang, Z. B. Direct Formation of Self-Assembled Nanoporous Aluminium Oxide on SiO_2 and Si Substrates. *Nanotechnology* **2002**, *13*, 627–630.
24. Tian, M. L.; Xu, S. Y.; Wang, J. G.; Kumar, N.; Wertz, E.; Li, Q.; Campbell, P. M.; Chan, M. H. W.; Mallouk, T. E. Penetrating the Oxide Barrier in Situ and Separating Freestanding Porous Anodic Alumina Films in One Step. *Nano Lett.* **2005**, *5*, 697–703.
25. Liang, J. Y.; Chik, H.; Yin, A. J.; Xu, J. Two-Dimensional Lateral Superlattices of Nanostructures: Nonlithographic Formation by Anodic Membrane Template. *J. Appl. Phys.* **2002**, *91*, 2544–2546.
26. Crouse, M. M.; Miller, A. E.; Crouse, D. T.; Ikram, A. A. Nanoporous Alumina Template with *In Situ* Barrier Oxide Removal, Synthesized from a Multilayer Thin Film Precursor. *J. Electrochem. Soc.* **2005**, *152*, D167–D172.
27. Coakley, K. M.; McGehee, M. D. Conjugated Polymer Photovoltaic Cells. *Chem. Mater.* **2004**, *16*, 4533–4542.
28. Zhang, Y.; Wang, C. W.; Rothberg, L.; Ng, M. K. Surface-Initiated Growth of Conjugated Polymers for Functionalization of Electronically Active Nanoporous Networks: Synthesis, Structure and Optical Properties. *J. Mater. Chem.* **2006**, *16*, 3721–3725.
29. Schierhorn, M.; Boettcher, S. W.; Ivanovskaya, A.; Norvell, E.; Sherman, J. B.; Stucky, G. D.; Moskovits, M. Fabrication and Electrochemical Photovoltaic Response of CdSe Nanorod Arrays. *J. Phys. Chem. C* **2008**, *112*, 8516–8520.
30. Que, W. X.; Uddin, A.; Hu, X. Thin Film TiO_2 Electrodes Derived by Sol-Gel Process for Photovoltaic Applications. *J. Power Sources* **2006**, *159*, 353–356.